NOTCH Signaling Limits the Response of Low-Grade Serous Ovarian Cancers to MEK Inhibition

Marta Llaurado Fernandez[1], E. Marielle Hijmans[2], Annemiek M.C. Gennissen[2], Nelson K.Y. Wong[1,3], Shang Li[4], G. Bea A. Wisman[5], Aleksandra Hamilton[1], Joshua Hoenisch[1], Amy Dawson[1], Cheng-Han Lee[1], Madison Bittner[1], Hannah Kim[1], Gabriel E. DiMattia[6], Christianne A.R. Lok[7], Cor Lieftink[2], Roderick L. Beijersbergen[2], Steven de Jong[4], Mark S. Carey[1], René Bernards[2], and Katrien Berns[2]

ABSTRACT

Low-grade serous ovarian cancer (LGSOC) is a rare subtype of epithelial ovarian cancer with high fatality rates in advanced stages due to its chemoresistant properties. LGSOC is characterized by activation of MAPK signaling, and recent clinical trials indicate that the MEK inhibitor (MEKi) trametinib may be a good treatment option for a subset of patients. Understanding MEKi-resistance mechanisms and subsequent identification of rational drug combinations to suppress resistance may greatly improve LGSOC treatment strategies. Both gain-of-function and loss-of-function CRISPR-Cas9 genome-wide libraries were used to screen LGSOC cell lines to identify genes that modulate the response to MEKi. Overexpression of *MAML2* and loss of *MAP3K1* were identified, both leading to overexpression of the NOTCH target *HES1*, which has a causal role in this process as its knockdown reversed MEKi resistance. Interestingly, increased *HES1* expression was also observed in selected spontaneous trametinib-resistant clones, next to activating *MAP2K1* (*MEK1*) mutations. Subsequent trametinib synthetic lethality screens identified *SHOC2* downregulation as being synthetic lethal with MEKis. Targeting SHOC2 with pan-RAF inhibitors (pan-RAFis) in combination with MEKi was effective in parental LGSOC cell lines, in MEKi-resistant derivatives, in primary ascites cultures from patients with LGSOC, and in LGSOC (cell line–derived and patient-derived) xenograft mouse models. We found that the combination of pan-RAFi with MEKi downregulated *HES1* levels in trametinib-resistant cells, providing an explanation for the synergy that was observed. Combining MEKis with pan-RAFis may provide a promising treatment strategy for patients with LGSOC, which warrants further clinical validation.

Introduction

Epithelial ovarian cancer is the most lethal gynecologic cancer worldwide. Low-grade serous ovarian cancer (LGSOC) is a relatively rare subtype, accounting for 5% of epithelial ovarian cancers and has distinct clinical and molecular features that differ from the more common high-grade serous ovarian cancer. LGSOC is characterized by indolent growth, young age at presentation, unresponsiveness to conventional chemotherapy, and activating mutations in MAPK signaling (1). Despite the slow growth of LGSOC, the presentation at advanced stage and resistance to conventional systemic treatments makes it ultimately a fatal disease. Therefore, better treatment options for patients with LGSOC are urgently needed.

Clinical studies on MEK inhibition in LGSOC were initiated based on the frequent identification of activating mutations in *KRAS*, *NRAS*, and *BRAF* in LGSOC (2). A phase II trial in LGSOC reported a 15% response rate to the MEK inhibitor (MEKi) selumetinib (3), which seemed to be a significant improvement over the reported response rate to conventional chemotherapy (4). A large phase III study (NCT01849874) of the MEKi binimetinib failed to show the benefit of this drug over chemotherapy in LGSOC. However, a *post hoc* analysis in patients with the *KRAS* mutation in this trial did suggest binimetinib benefit (5). Interestingly, recent reports on a phase II/III trial in recurrent LGSOC (NCT02101788) with the MEKi trametinib showed a response rate of 26% and a significant improvement in both progression-free survival and overall survival compared with standard therapies (6). These promising findings suggest that MEKi may become the new treatment option for a subset of patients with LGSOC.

Despite these encouraging results, experiences with targeted therapies over the past decades have taught us that both acquired and intrinsic resistance mechanisms often prevent long-term benefits, especially when given as single agents (7). Therefore, we aimed to identify MEKi-resistance mechanisms in LGSOC to optimize MEKi-based treatment strategies. For this, we performed genome-wide CRISPR/Cas9 functional genetic screens in cell lines established from patients with LGSOC (8). Furthermore, we generated spontaneous MEKi-resistant clones and analyzed the signaling pathways involved in their resistance.

[1]Department of Obstetrics and Gynaecology, University of British Columbia Vancouver, British Columbia, Canada. [2]Division of Molecular Carcinogenesis, Oncode Institute, Cancer Genomics Center Netherlands, the Netherlands Cancer Institute, Amsterdam, the Netherlands. [3]Department of Experimental Therapeutics, BC Cancer, Vancouver, British Columbia, Canada. [4]Department of Medical Oncology, Cancer Research Center Groningen, University of Groningen, University Medical Center Groningen, Groningen, the Netherlands. [5]Department of Gynecologic Oncology, Cancer Research Center Groningen, University of Groningen, University Medical Center Groningen, Groningen, the Netherlands. [6]Mary and John Knight Translational Ovarian Cancer Research Unit, London Health Sciences Center. [7]Center for Gynecologic Oncology Amsterdam, Antoni van Leeuwenhoek/The Netherlands Cancer Institute, Amsterdam, the Netherlands.

M. Llaurado Fernandez, E.M. Hijmans, and A.M.C. Gennissen contributed equally to this work.

Corresponding Authors: Katrien Berns, Plesmanlaan 121, 1066 CX Amsterdam, the Netherlands. Phone: 31-20-5121955. E-mail: k.berns@nki.nl; and Mark S. Carey, Vancouver, British Columbia V6Z 2K8, Canada. Phone: 160-4875-4268; E-mail: mark.carey@ubc.ca; René Bernards, Plesmanlaan 121,1066 CX Amsterdam, the Netherlands. Phone: 31-20-5121952; E-mail: r.bernards@nki.nl

Mol Cancer Ther 2022;21:1862–74

doi: 10.1158/1535-7163.MCT-22-0004

Our work reveals a previously unrecognized signaling pathway as critically involved in MEKi resistance, which suggests a combination strategy for patients with LGSOC.

Materials and Methods

Cell lines and culture

VOA-3723, VOA-4627, and VOA-6406 (RRID:CVCL_VQ52) cells were established by the Mark Carey lab (8, 9). The iOvCa241-PAR and iOvCa241-RES (selected under 20 nmol/L trametinib) cells were provided by the Gabriel DiMattia lab. All cells were maintained in DMEM (Gibco) supplemented with 10% FBS and 100 μg/mL penicillin/streptomycin and 2 mmol/L L-glutamine (Gibco). For primary ascites cultures, 25-mL fresh ascites was combined with 25-mL OSE medium in a T175 flask until confluency. The OSE medium (Wisent Bio Products) was supplemented with 10% FBS, 2.5 μg/mL amphotericin B (Thermo Fisher), and 50 μg/mL gentamicin (Sigma; ref. 10). For the ascites cultures, written informed consent was obtained in accordance with the declaration of Helsinki, and the use was approved by our institutional review board. The ascites cultures proliferated only a few passages. Further authentication of the obtained cell lines was not performed. *RAS* mutation status of the VOA-6406 and IOvCa241 cell lines was confirmed by Sanger sequencing. All cultures were frequently checked for Mycoplasma using a qPCR-based method.

CRISPR-CAS9 genome-wide screens

For the overexpression screen, we introduced two components of the Synergistic Activation Mediator (SAM) complex into the cells: the inactive Cas9-VP64 fusion and the MS2-P65-HSF1 helper protein creating VOA-6406/dCas9MS2. VOA-6406/dCas9MS2 cells were transduced with the genome-wide CRISPR/Cas9 SAM library, consisting of 70,290 guides (activating 23,430 coding isoforms; ref. 11; Addgene No. 1000000057). For the knockout enhancer/resistance screen, cells were transduced with the genome-wide CRISPR/Cas9 Brunello sgRNA library in backbone lentiCRISPRV2 containing 76,441 unique sgRNAs (targeting 19,114 genes) along with 1,000 nontargeting controls (ref. 12; Addgene No. 73179). For the resistance screens, cells were transduced at a multiplicity of infection below 0.5 and 250× representation of each guide; for the enhancer screen, 1,000× representation of the guides was maintained. After 4 to 5 days of zeocin or puromycin selection and recovery, cells were trypsinized, counted, a t0 sample was taken, and the transduced cells were plated in the absence (untreated, ut) or presence (treated, tr) of trametinib (5 nmol/L for resistance screen, 2 nmol/L for enhancer screen). The medium was replaced every 3 days, and the screens were all performed in triplicate. For the resistance screens, cells were harvested after 3 to 4 weeks, for the enhancer screen after 10 days, and genomic DNA was isolated using a ZYMO gDNA isolation kit according to the manufacturer's protocol. sgRNAs were amplified using a capture/two-step PCR protocol for next-generation sequencing in an Illumina HiSeq-2500 as described (13). sgRNA abundance in treated and untreated samples was analyzed using DESeq2 (RRID:SCR_000154) and RRA MAGeCK tools (refs. 14, 15). For sequence depth normalization, a relative total size factor was calculated for each sample, by dividing the total counts of each sample by the geometric mean of all totals as described (16). After normalization, a differential test between the treated and untreated condition for each sgRNA was performed using DESeq2, and the output was sorted in a specific order depending on the interest: depletion or enhancement. We used the MAGeCK Robust Rank Algorithm to determine for each gene whether its sgRNAs were enriched toward the top of the result list. The resulting enrichment *P* values were corrected for multiple testing using the Benjamini–Hochberg correction, resulting in a false-discovery rate (FDR)-corrected value. Raw data of the screens are provided in Supplementary Files S1–S3 and have been deposited in NCBI's Gene-Expression Omnibus accessible through GEO series accession number GSE213580 (https://www.ncbi.nlm.nih.gov/geo/query/acc.cgi?acc=GSE213580).

Plasmids and guide sequences

The lentiviral vectors pcw107-NOTCH-IC-V5 and pLKO.1-Scramble shRNA (sh*CTRL*) were obtained from Addgene (No. 64622 and No. 1864). The doxycycline-inducible sh*SHOC2* pZIP-TRE3G lentiviral vector was purchased from TransOMIC (No. TLHVU2310). The following TRC pLKO.1 shRNA vectors were used:

SHOC2 No. 1: TRCN0000153425;
SHOC2 No. 2: TRCN0000151223;
HES1 No. 3: TRCN0000018991;
MAP3K1: TRCN0000006159.

The following guides were cloned into pLenti-CRISPRv2.1 (Addgene No. 52961);

gCTRL No. 1 (chrom 5): GGAACTTAACTGAGAACAAG
gCTRL No. 2 (chrom 9): GATGAACAGATTAAGAATGA
g*MAP3K1* No. 1: ATCTGCACATTTGACTAGGA
g*MAP3K1* No. 2: CTTCTCACCATATAGCCCTG
g*MAP2K4*: TATCCTTGTCGTGATGCGCT

The following guides were cloned into pSAM1.2:

gSAM-*MAML2* No. 1: AGAGCTCGTTCGAGGCTCCC
gSAM-*MAML2* No. 2: AGTGGCACCAGCCTTCCACC

Combination index

Cells were plated in white-walled 384-well plates (Greiner) at predetermined optimal density. After cells were attached, drugs were added using the Tecan D300e digital dispenser. A total of 10 μmol/L phenylarsine oxide (PAO) was used as a positive control and DMSO as a negative control. Cell viability assays were performed using CellTiter-Glow (Promega) according to the manufacturer's instructions and measured in the Envision (Perkin Elmer). Growth assays were plated as multiple measurements in the 384 plates (at least quadruple) and performed several times (at least three times). Measurements were normalized to the positive and negative controls. Combination index (CI) synergy scores were calculated as described (17), and displayed are the median CI scores from the synergy matrix (5 × 5 concentration range matrix, with twofold dilution steps). CI scores are defined as <0.1 very strong synergism; 0.1 to 0.3 strong synergism; 0.3 to 0.7 synergism; 0.7 to 0.85 moderate synergism; and 0.85 to 0.9 slight synergism.

Antibodies and compounds

For Western blotting, primary antibodies against MAP3K1 (sc-17820, RRID:AB_627926), CK7 (sc-23876), HES1 (sc-25392, RRID:AB_647996), HSP90 (sc-13119), CDKN1C (sc-1039, sc-1037), and pY204ERK (sc-7383) were obtained from Santa Cruz Biotechnology; ACTIN (No. 3700), ERK (No. 4695), JUN (No. 2315), pS73JUN (No. 3270), PAX8 (No. 59019), RSK (No. 8408), pT359RSK (No. 8753), SHOC2 (No. 53600), cleaved NOTCH1 (No. 2421), NOTCH2 (No. 4530), NOTCH3 (No. 5276), and NOTCH4 (No. 2423) were from Cell Signaling Technology and MAML2 (A300-682) was obtained from Bethyl Laboratories. Secondary antibodies Goat anti-Rabbit IgG-HRP conjugate (No. 1706515) and Goat anti-Mouse IgG–HRP conjugate (No. 1706516) were purchased from Bio-Rad. Trametinib (No. 201458; ref. 18), LY3009120 (No. 206161; ref. 19), and ABT-263 (No. 201970; ref. 20) were purchased from Medkoo Biosciences. BGB-283 (No. S7926; ref. 21), JI051 (No. S0483;

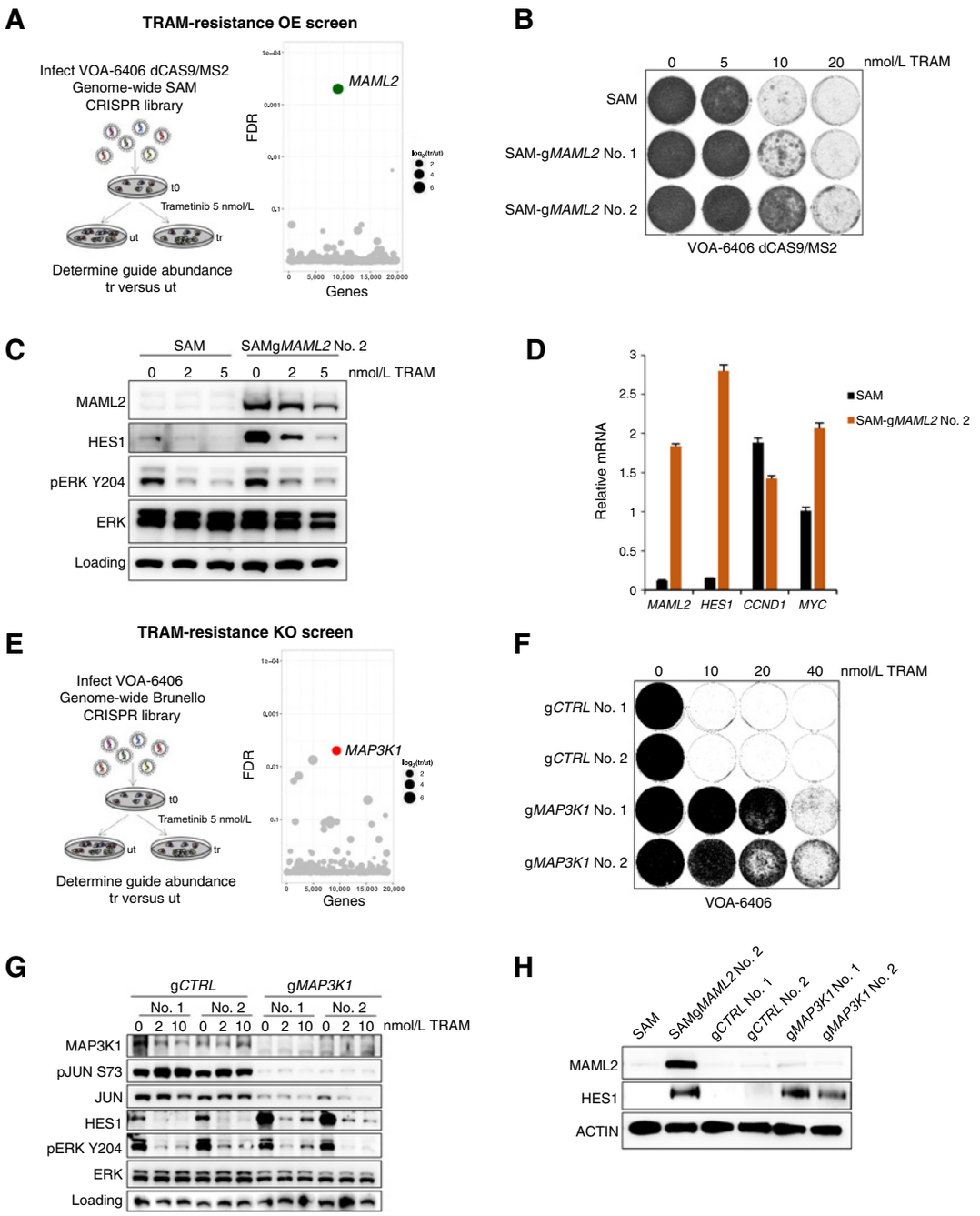

Figure 1.

Genome-wide trametinib-resistance screen identifies *MAML2* and *MAP3K1*. **A,** Overview of genome-wide trametinib resistance screen in VOA-6406dCas9MS2 cell line with the SAM library targeting 23,430 isoforms for transcriptional activation. Cells were infected with MOI below 0.5 and 250× representation of guides. Trametinib selection was performed for 3 weeks, after which gRNA abundance was determined in treated (tr) over untreated (ut) conditions through deep sequencing. Screens were performed in triplicate. Validated hit *MAML2* is highlighted in the bubble plot presentation of the DESeq2/ RRA MAGeCK analysis. FDR threshold <0.1. **B,** The functional phenotypes of lentiviral SAM1.2-g*MAML2* vectors (No. 1 and No. 2) in the VOA-6406 dCas9MS2 cell line upon trametinib treatment was measured in a long-term colony-formation assay. Cells expressing an empty pSAM1.2 vector were used as control. The cells were fixed, stained, and scanned after 14 days. **C,** Western blot analysis of the VOA-6406 dCas9MS2 cell line transduced with lentiviral SAM1.2 and SAM1.2-g*MAML2 No.*2 and exposed to 0, 2, and 5 nmol/L trametinib for 3 days. Blots were probed with the indicated antibodies. HSP90 was used as a loading control. **D,** VOA-6406dCas9MS2 cells transduced with SAM1.2 and SAM1.2g*MAML2* No. 2 were subjected to mRNA expression analysis with QRT-PCR. mRNA levels were normalized to the expression of GAPDH and displayed is the relative expression of the indicated mRNAs. Error bars denote SD. **E,** Overview of genome-wide trametinib-resistance screen in VOA-6406 cell line with the Brunello library targeting 19,114 genes. Cells were infected with MOI below 0.5 and 250× representation of guides. (*Continued on the following page.*)

ref. 22), palbociclib (No. S1116; ref. 23), selumetinib (No. S1008; ref. 24), refametinib (No. S1089; ref. 24), and trametinib (No. S2673 used in the cell viability assays from Supplementary Fig. S2C) were purchased from Selleck Chemicals. NVPBEZ235 (No. 1281; ref. 25) and RO4929097 (No. 2521; ref. 26) were purchased from Axon Medchem. DAPT (No. HY13027; ref. 27) was purchased from MedChemExpress.

LGSOC xenograft and patient-derived xenograft models

The VOA-6406 xenograft model was established by the initial subcutaneous inoculation of VOA-6406 parental cells in NRG mice. VOA-6406 tumor pieces ($1 \times 2 \times 2$ mm^3) were harvested from actively growing tumors and were implanted subcutaneously in NRG mice. Because VOA-6406 tumors were cystic, the tumors were harvested with the exclusion of the cystic fluid, which is presented as the "dry weight." LGSOC patient-derived xenograft (PDX) models were established as described previously (28) and patients gave written informed consent. *RASG13D*-mutant PDX OC.79 was obtained from a FIGO stage IIIC patient with LGSOC treated with adjuvant carboplatin/paclitaxel chemotherapy. F3 tumor pieces from the OC.079 PDX model were cut into $3 \times 3 \times 3$ mm^3 pieces and subcutaneously implanted in NSG mice. The *RAS/RAF* WT PDX model AB743 was developed from a recurrent FIGO stage III patient with LGSOC treated with tamoxifen. Actively growing AB743 PDXs were harvested and cut into pieces of $1 \times 2 \times 2$ mm^3 and subcutaneously implanted in NRG mice.

When the tumors demonstrated sustained growth with a tumor size of 100 to 150 mm^3, the mice were assigned into vehicle control or treatment groups ($n = 5$–7 tumors/group). Endpoint of the treatments was either tumor volume of 1,500 mm^3, >15% weight loss, or 5 to 6 weeks of treatment (for the slow-growing OC.079 model 57 days). For all models, drug combinations were formulated in DMSO: Kolliphor EL (Sigma 27963): saline solution, in a 1:1:8 ratio. Mice were treated 5 days a week (Monday to Friday) at the indicated doses by intraperitoneal injection. Tumor growth was quantified twice a week (VOA-6406 and PDX AB743) or every day (PDX OC.79) by caliper measurements according to the formula: (width^2 × length)/2. Relative tumor growth was determined as tumor volume on treatment day/tumor volume at the start of treatment. Statistical significance for tumor weight differences was determined using a two-tailed *t* test, for survival differences log-rank (Mantel–Cox) test. The animal studies with VOA-6406 xenografts and PDX model AB743 were carried out at Animal Resources Centre at BC Cancer, Vancouver, according to animal ethics certificate A18-0105 approved by the Animal Care Committee at the University of British Columbia. The animal studies with PDX OC.79 were carried out at Animal Facility Cancer Research Centre Groningen, according to guidelines and approved by the Institutional Animal Care and Use Committee of the University of Groningen.

Additional methods

Lentivirus production, Western blots, proliferation and viability assays, and qRT-PCR primers are described in the Supplementary Methods.

Data availability statement

The data generated in this study are generated by the authors and are available within the article and its supplementary files.

Results

Genome-wide gain-of-function MEKi-resistance screen in LGSOC

To identify genes implicated in MEKi response in LGSOC, we performed a genome-wide CRISPR/dCas9-mediated overexpression screen in the LGSOC cell line VOA-6406. The cell line VOA-6406 was chosen from a panel of well-characterized LGSOC cell lines, based on its partial MEKi sensitivity and the presence of an *NRAS* mutation (9). For the screen, we made use of the human CRISPR/dCas9 SAM library, which is a pooled library, that uses an engineered protein complex for the transcriptional activation of genes (11). The SAM library was introduced into VOA-6406/dCas9MS2 cells, and after 3 weeks of selection with the MEKi trametinib (5 nmol/L), cells were harvested and single-guide RNA (sgRNA) abundance was determined, which identified one clear outlier: *MAML2* (**Fig. 1A**). In a validation experiment, we showed that MAML2 overexpression by the introduction of either sg*MAML2* No. 1 or sg*MAML2* No. 2 induced trametinib resistance in a long-term proliferation assay (**Fig. 1B**). The more pronounced resistance caused by sg*MAML2* No. 2 compared with sg*MAML2* No. 1 is a consequence of its ability to enhance higher endogenous MAML2 transcription (Supplementary Fig. S1A and S1B). MAML2 acts as a transcriptional coactivator of NOTCH proteins, and MAML2 overexpression is expected to amplify NOTCH-induced transcription. We observed increased protein and mRNA levels of the NOTCH target gene *HES1* upon MAML2 overexpression (**Fig. 1C** and **D**; Supplementary Fig. S1C). For two other NOTCH target genes, *CCND1* and *MYC*, the effect of MAML2 overexpression was absent or modest (**Fig. 1D**), indicating that *HES1* mRNA or protein levels appear the best readout for NOTCH activation in these cells.

Genome-wide loss-of-function MEKi-resistance screen in LGSOC

To further identify genes implicated in MEKi response in LGSOC, we performed a genome-wide CRISPR/Cas9-mediated knockout screen in the cell line VOA-6406. For the knockout screen, we transduced the genome-wide lentiviral Brunello library into VOA-6406 cells. After 3 to 4 weeks of trametinib (5 nmol/L) selection, cells were harvested, sgRNA sequences were amplified and subjected to deep-sequence analysis. The results revealed that gRNAs targeting *MAP3K1* were most significantly enriched in this screen (**Fig. 1E**). For follow-up validation experiments, we generated monoclonal *MAP3K1* knockout cell lines from two independent gRNA transductions, denoted sg*MAP3K1* No. 1 and sg*MAP3K1* No. 2. As expected, both monoclonal *MAP3K1* knockout lines displayed trametinib-resistance compared with the control lines (**Fig. 1F**; Supplementary Fig. S1D) and

(*Continued.*) Trametinib selection was performed for 3 weeks, after which gRNA abundance was determined in treated (tr) over untreated (ut) conditions through deep sequencing. Screens were performed in triplicate. Validated hit *MAP3K1* is highlighted in the bubble plot presentation of the DEseq2/ RRA MAGeCK analysis. FDR threshold <0.1. **F,** Colony-formation assays were performed with selected VOA-6406 monoclonal cell lines transduced with g*CTRL* No. 1 (nontargeting region in chromosome 5), g*CTRL* No. 2 (nontargeting region in chromosome 9), and g*MAP3K1* No. 1 and g*MAP3K1* No. 2. Plated cells were exposed to increasing trametinib concentrations as indicated. The cells were fixed, stained, and scanned after 10 days. Colony-formation assays were performed in triplicate, and a representative staining is shown. **G,** Western blot analysis of total lysates generated from the monoclonal g*CTRL* (No. 1 and No. 2) and g*MAP3K1* (No. 1 and No. 2) lines exposed to 0, 2, and 10 nmol/L trametinib for 1 day. Blots were probed with the indicated antibodies. **H,** Western blot analysis of the VOA-6406 dCas9MS2 cell line transduced with lentiviral SAM1.2 and SAM1.2-g*MAML2 No.* 2 and the VOA-6406 monoclonal lines g*CTRL* (No. 1 and No. 2) and g*MAP3K1* (No. 1 and No. 2). Blots were probed with the indicated antibodies.

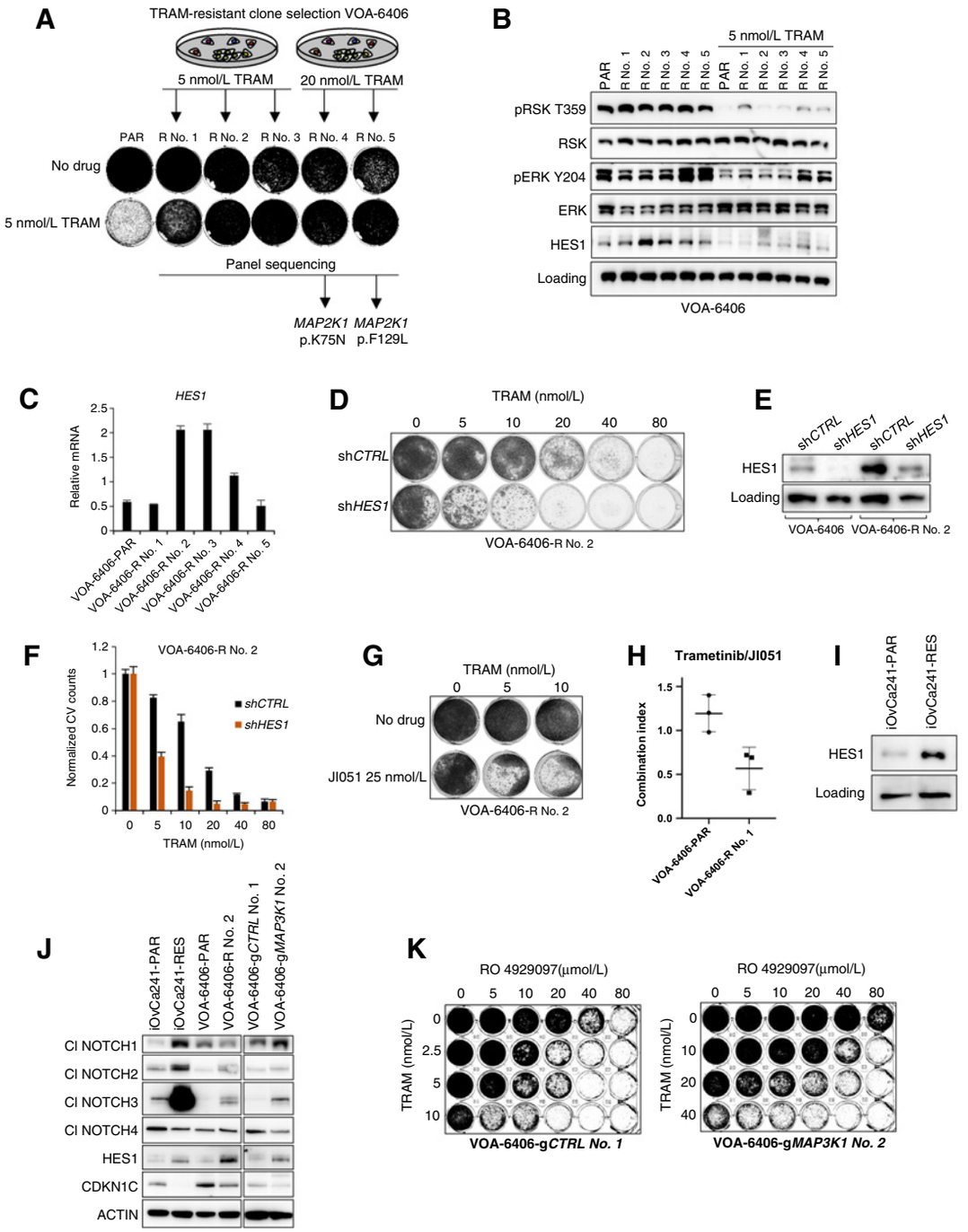

Figure 2.

Spontaneous trametinib resistance through *MAP2K1* mutation or *HES1* upregulation. **A,** VOA-6406 cells were plated at low density, and spontaneous trametinib-resistant clones were selected by 4 to 6 weeks of exposure to 5 or 20 nmol/L trametinib as indicated. Selected clones were subjected to targeted sequence analysis of 178 cancer-associated genes (NKI-178 panel). **B,** Western blot analysis of total lysates generated from the parental VOA-6406 (PAR) and the monoclonal VOA-6406 R No. 1, R No. 2, R No. 3, R No. 4, and R No. 5 lines exposed to 5 nmol/L trametinib for 2 days. Blots were probed with the indicated antibodies. HSP90 was used as a loading control. **C,** The parental VOA-6406 (PAR) and monoclonal VOA-6406 R No. 1, R No. 2, R No. 3, R No. 4, and R No. 5 lines were subjected to mRNA expression analysis with QRT-PCR. mRNA levels of *HES1* were normalized to the expression of GAPDH, and displayed is the relative expression in the indicated monoclonal trametinib-resistant lines. Error bars, SD. **D,** Colony-formation assays were performed with the VOA-6406-R No. 2 line, which was infected with sh*CTRL* (scrambled hairpins) and sh*HES1* constructs. Stably selected cells were exposed to increasing trametinib concentrations as indicated. The cells were fixed, stained, and scanned after 11 days. Colony-formation assays were performed in triplicate, and a representative staining is shown. **E,** Western blot analysis of total lysates generated from the sh*CTRL*- and sh*HES1*-transduced VOA-6406 and VOA-6406-R No. 2 lines. Blots were probed with HES1 and HSP90 (loading control) antibodies. (*Continued on the following page.*)

lost MAP3K1 protein expression (**Fig. 1G**; Supplementary Fig. S1E and S1F). Furthermore, we could show that *MAP3K1* loss in an independent LGSOC line VOA-3723 (8) also resulted in trametinib resistance, suggesting a common underlying mechanism (Supplementary Fig. S1G). MAP3K1 has been implicated in JNK and MAPK signaling previously (29). Signaling analysis in the g*MAP3K1* clones demonstrated that loss of MAP3K1 protein impaired JNK/JUN signaling, without any effect on MAPK signaling (**Fig. 1G**). Moreover, we identified that the loss of *MAP2K4*, which is downstream in the MAP3K1 signaling cascade, resulted in MEKi resistance (Supplementary Fig. S1H). We conclude that *MAP3K1* loss contributes to trametinib resistance via its canonical downstream signaling but without any rebound of the MAPK signaling cascade.

To understand the mechanism of MEKi resistance upon *MAP3K1* loss, we tested whether *MAP3K1* loss mimics MAML2 overexpression by engagement of nodes in the NOTCH signaling cascade, such as HES1 upregulation. We observed increased protein levels of the NOTCH target HES1 in both g*MAP3K1* monoclonal lines, similar to what was observed upon MAML2 overexpression (**Fig. 1G** and **H**). Furthermore, overexpression of the active form of NOTCH1 (NOTCH-NICD) induced *HES1* transcription and dampened trametinib response in the VOA-6406 cell line, demonstrating that activated NOTCH signaling is sufficient to bypass a trametinib-induced arrest (Supplementary Fig. S1I–S1K). Our data show that two independent genome-wide resistance screens revealed pathways leading to overexpression of the NOTCH target HES1.

Spontaneous MEKi resistance via MAP2K1 (MEK1) mutation or HES1 induction

Next, we asked whether the resistance mechanism identified through CRISPR/Cas9 screening may also occur during the development of spontaneous MEKi resistance. To investigate this, VOA-6406 cells were exposed to either 5 nmol/L or 20 nmol/L trametinib, and spontaneously resistant clones were isolated after 6 to 8 weeks (**Fig. 2A**). From the 5 nmol/L condition, multiple resistant clones were recovered from which R No. 1, R No. 2, and R No. 3 were selected for further analysis. In the 20 nmol/L condition, only two clones (R No. 4 and R No. 5) demonstrated sustained growth under the higher trametinib concentration. First, we panel-sequenced the five clones for 178 cancer-associated genes (30). We only found mutations in the 20 nmol/L trametinib-selected clones R No. 4 and R No. 5, and identified *MAP2K1*p.K75N and *MAP2K1*p.F129 L, respectively. The *MAP2K1*p.F129 L mutation was further verified by Sanger sequencing (Supplementary Fig. S2A). The *MAP2K1*p.F129 L mutation has been implicated in MEKi resistance previously and is suggested to enhance MEK/RAF interaction and has increased intrinsic kinase activity (31). We observed higher MAPK signaling in both R No. 4 and R No. 5 clones, and sustained MAPK signaling in the presence of trametinib (**Fig. 2B**). Resistant clone R No. 5 displayed trametinib resistance in long-term proliferation assays (Supplementary Fig. S2B) and displayed resistance to the four MEKis, trametinib, selumetinib, binimetinib, and refametinib (Supplementary Fig. S2C). The R No. 5 clone also displayed some form of drug addiction, as culturing in the absence of MEKis slowed the proliferation of this clone, probably caused by toxic high levels of MEK activity in these cells in the absence of the drug. Sequencing the cancer gene panel in the clones selected under 5 nmol/L trametinib did not reveal any acquired mutations. For the VOA-6406-R No. 1 clone, we observed a mild MAPK rebound signaling upon trametinib exposure, but at present, we have not identified the underlying resistance mechanism. In the clones R No. 2 and R No. 3, no rebound of MAPK signaling was observed, but similar to our previous identified resistance mechanism, these clones displayed elevated *HES1* levels, both in terms of protein and RNA (**Fig. 2B** and **C**). Notably, the R No. 2 and R No. 3 trametinib resistance phenotype appeared to be reversible. Upon prolonged culturing in the absence of drug, the clones lost their resistance phenotype, suggestive of a transient switchable (epigenetic) resistance mechanism (Supplementary Fig. S2D). To test the importance of elevated *HES1* levels in the spontaneous resistant clones, *HES1* levels were downregulated in the R No. 2 clone with an sh*HES1* construct. Knockdown of *HES1* resulted in trametinib sensitization in the R No. 2 clone, which suggested an acquired dependency on elevated *HES1* levels in these cells (**Fig. 2D**–**F**). Furthermore, we tested the compound JI051, which has been described to inhibit HES1, by stabilizing the (inactive) interaction between prohibitin2 (PHB2) and HES1 (22). The JI051 compound dampened the trametinib resistance of the VOA-6406-R No. 2 spontaneous resistant clone when applied in combination (**Fig. 2G**). Furthermore, CI measurements indicated synergy of the trametinib/JI051 combination primarily in the R No. 2 clone (**Fig. 2H**). Similarly, knockdown of *HES1* levels or HES1 inhibition with JI051 resensitized the trametinib-resistant *MAP3K1* knockout clone to trametinib inhibition, further demonstrating a critical role for HES1 levels in trametinib resistance (Supplementary Fig. S2E and S2F). We also identified elevated HES1 levels in an independently selected trametinib-resistant clone in the LGSOC line iOvCa241 (8), suggesting a common trametinib escape route mechanism (**Fig. 2I**). Furthermore, in all of the cell line pairs tested, the trametinib-resistant subclones displayed elevated levels of cleaved NOTCH family members, most notably NOTCH3, and to a lesser extent NOTCH1 and NOTCH2. This induction of NOTCH cleavage may be responsible for the induced HES1 levels observed in these trametinib-resistant subclones. Repression of CDKN1C was used as a readout of HES1 activity (**Fig. 2J**). How the resistant clones upregulate NOTCH cleavage is still under investigation. Our findings suggest that inhibition of NOTCH cleavage by the addition of gamma-secretase inhibitors may enhance trametinib efficacy in LGSOC cells. Combination treatment of VOA-6406-g*CTRL* No. 1 and VOA-6406-g*MAP3K1* No. 2 with the gamma-secretase inhibitors RO4929097 and DAPT caused synergistic trametinib-induced proliferation arrest and *HES1* mRNA downregulation (**Fig. 2K**; Supplementary Fig. S3A–S3F). However, the concentrations of the gamma-secretase inhibitors needed to achieve NOTCH pathway inhibition in the LGSOC cells were high. It is questionable whether such high concentrations can be reached and tolerated *in vivo* (32).

(*Continued.*) **F,** Crystal violet quantification of colony-formation assays performed as described in **D**. Displayed are the relative values compared with untreated condition. Error bars, SD. **G,** Colony-formation assays were performed with VOA-6406-R No. 2 incubated in the presence of trametinib (0, 5, 10 nmol/L) and/or the HES inhibitor JI051 (25 nmol/L) as indicated. The cells were fixed, stained, and scanned after 10 days. **H,** CI were calculated for the trametinib/JI051 combination in parental VOA-6406 and VOA-6406-R No. 2. All 384-well growth assays were performed multiple times and were normalized to positive (POA) and negative (DMSO) controls. Displayed are the median CI values of the synergy 5 × 5 concentration matrix. Error bars, SD. Values below 0.9 indicate synergy. **I,** Western blot analysis of total lysates generated from parental (PAR) and TRAM-resistant (RES) subclones derived from iOvCa241 by prolonged TRAM (20 nmol/L) exposure. Blots were probed with the indicated antibodies. HSP90 was used as a loading control. **J,** Parental and TRAM-resistant cell line pairs were plated at equal densities, and the next day, total lysates were subjected to Western analysis with the indicated antibodies. **K,** Colony-formation assays were performed in VOA-6406-g*CTRL* No. 1 and VOA-6406-g*MAP3K1* No. 2 with increasing (combination) dosage of trametinib and the gamma-secretase inhibitor RO4929097 as indicated. The cells were fixed, stained, and scanned after 7 days. Colony-formation assays were performed in triplicate, and a representative staining is shown.

We conclude that, in spontaneous trametinib resistance in LGSOC, besides acquisition of activating *MAP2K1* (*MEK1*) mutations, the elevation of HES1 protein levels appears to be a common mechanism. These results suggest that increased *HES1* is a critical and general component of the trametinib resistance, and targeting HES1 may provide a strategy to enhance MEKi responsiveness.

Genome-wide MEKi synthetic lethality screen in LGSOC

Next, we sought to further explore trametinib combination strategies to prevent the development of resistance. For this, we performed a trametinib synthetic lethality screen in the LGSOC VOA-4627 line, a cell line with intrinsic trametinib resistance and already elevated HES1 levels (Supplementary Fig. S1J; ref. 8). The optimal screening dose (a trametinib concentration that hardly affected proliferation) was determined at 2 nmol/L trametinib. Next, VOA-4627 cells were transduced with the genome-wide lentiviral Brunello CRISPR library, and stably infected cells were divided into control (ut) and trametinib 2 nmol/L (tr) conditions. After 10 days, sgRNA abundance was determined (**Fig. 3A**). Several hits were identified from which *SHOC2* performed best in subsequent validation experiments (**Fig. 3B** and **C**). *SHOC2* depletion was recently identified to be synthetic lethal with MEK inhibition in other RAS-driven cancers, suggesting a synthetic lethal interaction across multiple tumor types (33). Mechanistically, it has been proposed that *SHOC2* deletion prevents MEKi-induced RAF dimerization, thereby leading to more potent pathway inhibition (34). Upon further validation in a doxycycline-inducible sh*SHOC2* cell line, we could show that *SHOC2* knockdown enhances trametinib efficacy in VOA-6406 cells (**Fig. 3D** and **E**). Because no SHOC2 inhibitors have been developed to date, we aimed to mimic *SHOC2* depletion by using the pan-RAF inhibitor LY3009120, which has been reported to efficiently inhibit RAF dimers (35). In the doxycycline-inducible sh*SHOC2* VOA-6406 cell line, we could demonstrate that MEKi/LY3009120 has similar growth inhibitory properties to MEKi/*SHOC2* depletion. Furthermore, the addition of LY3009120 has no further growth inhibitory effects under *SHOC2*-depleted conditions giving support for the notion that both LY3009120 and *SHOC2* loss target the same node (**Fig. 3F**). When testing the combination of trametinib and LY3009120 in several parental LGSOC lines (VOA-3723, VOA-4627, and VOA-6406), spontaneous resistant clone VOA-6406R No. 1, spontaneous HES1-mediated resistant clone VOA-6406-R No. 2, and a resistant *MAP2K1*-mutant clone VOA-6406-R No. 5, we observed synergy in long-term proliferation assays (**Fig. 3G**). To quantify the extent of synergy, CI were calculated over a matrix of trametinib and LY3009120 combinations and the mean of the CI matrix indicated synergy in all the lines tested, with the best synergy score (CI = 0.3) in the spontaneous resistant clone VOA-6406-R No. 2 (**Fig. 3H**). To put our findings in context, we compared our trametinib/LY3009120 combination to other suggested trametinib combination strategies such as trametinib combined with CDK4/6i (palbociclib), BCL2/Xli (ABT-263), and PI3K/MTORi (NVPBEZ235). We found only synergy with the trametinib/LY3009120 combination in the LGSOC cell line VOA-4627 (Supplementary Fig. S3G; refs. 36, 37).

To ensure the general applicability of MEKi/pan-RAFi combination, we also tested an independent pan-RAFi, BGB283 (lifirafenib; ref. 21). Similar to LY3009120, BGB283 in combination with trametinib resulted in synergistic inhibition of proliferation in both the parental VOA-6406 and the resistant clone R No. 2, the parental iOvCa241-PAR and trametinib-resistant subclone iOvCa241-RES, and the VOA-6406 control and *MAP3K1*-knockout clone (**Fig. 4A–F**; Supplementary Fig. S4A–S4C). To test the reversibility of the MEKi/pan-RAFi combination, VOA-6406 cells were exposed for 1 week to the combination, after which cells were washed and cultured without drugs for 3 weeks. We observed no reversal of the growth arrest in the combination treatment, whereas resistant colonies grew out in the single-drug treatments (**Fig. 4G**). For all of the cell line pairs, the addition of pan-RAFi to trametinib resulted in a further decrease in MAPK pathway activity. In addition, we observed HES1 downregulation upon the MEKi/pan-RAFi combination treatment (**Fig. 4H** and **I**). Given the critical role of elevated HES1 in the trametinib-resistance phenotypes, we suggest that the combined effect of MEKi/pan-RAFi on HES1 levels may contribute to their synergistic interaction.

Validation of MEKi/pan-RAFi combination in primary ascites cultures

The scarcity and slow growth characteristics of LGSOC make it challenging to grow cell line xenografts or PDXs in mice. As an alternative, we generated primary ascites cultures from patients with LGSOC to allow direct testing of the MEKi/pan-RAFi combination in LGSOC. We managed to establish primary ascites cultures from chemo-naïve patients with LGSOC whose ascites was removed during cytoreductive surgery or to relieve clinical symptoms (**Fig. 5A**; Supplementary Fig. S5A). As quality control, ascites-derived cultures were stained with the LGSOC markers PAX8 and CK7 to ensure the Müllerian/epithelial origin of the cells (**Fig. 5B**). The primary ascites cultures proliferated for a few passages, which allowed us to test the trametinib/LY3009120 combination in proliferation assays. We observed that the primary ascites cultures responded with either moderate or strong proliferation arrest with the MEKi/pan-RAFi combination (**Fig. 5C**), with a clearly visible reduction in cell viability (**Fig. 5D**). To extend our previous MEKi synthetic lethality screen findings, we induced *SHOC2* knockdown in the ascites culture KAM004A. Knockdown of *SHOC2* resulted in decreased levels of pERK Y204 and HES1, which were further decreased in combination with trametinib, similar to our MEKi/pan-RAFi combination findings in the established LGSOC cell lines (**Fig. 5E**). In agreement with previous observations, combined MEKi/pan-RAFi treatment resulted in HES1 and MAPK pathway inhibition in the primary ascites culture KAM010A (**Fig. 5F** and **G**; Supplementary Fig. S5B). Collectively, the data obtained in established LGSOC cell lines appeared similar in primary ascites cultures from patients with LGSOC. These results warrant further exploration of a MEKi/pan-RAFi combination treatment strategy in LGSOC.

In vivo validation of the MEKi/pan-RAFi combination

Despite the general difficulties with establishing *in vivo* LGSOC mouse models, we managed to develop a xenograft transplantation model based on VOA-6406 in NRG mice, which was used to test the trametinib/BGB283 combination treatment strategy. We observed no effect of single BGB283 treatment at 5 mg/kg dosing and some effect of the BGB283 10 mg/kg concentration (**Fig. 6A**). The tumors appeared already quite responsive to trametinib single treatment (TRAM 0.5 mg/kg), although a heterogeneous response was observed, where two of five trametinib-treated tumors showed a more than 30% reduction in tumor size (**Fig. 6B**). The combination treatment (BGB283 5 mg/kg + TRAM 0.5 mg/kg) was superior to the single treatments, as six of six of the combination-treated tumors displayed a more than 30% tumor volume reduction by day 33 (**Fig. 6B**). Furthermore, the combination treatment resulted in significant reduction in dry tumor weights (TRAM vs. BGB283 + TRAM $P = 0.0089$*t*, test two-tailed; Supplementary Fig. S6A).

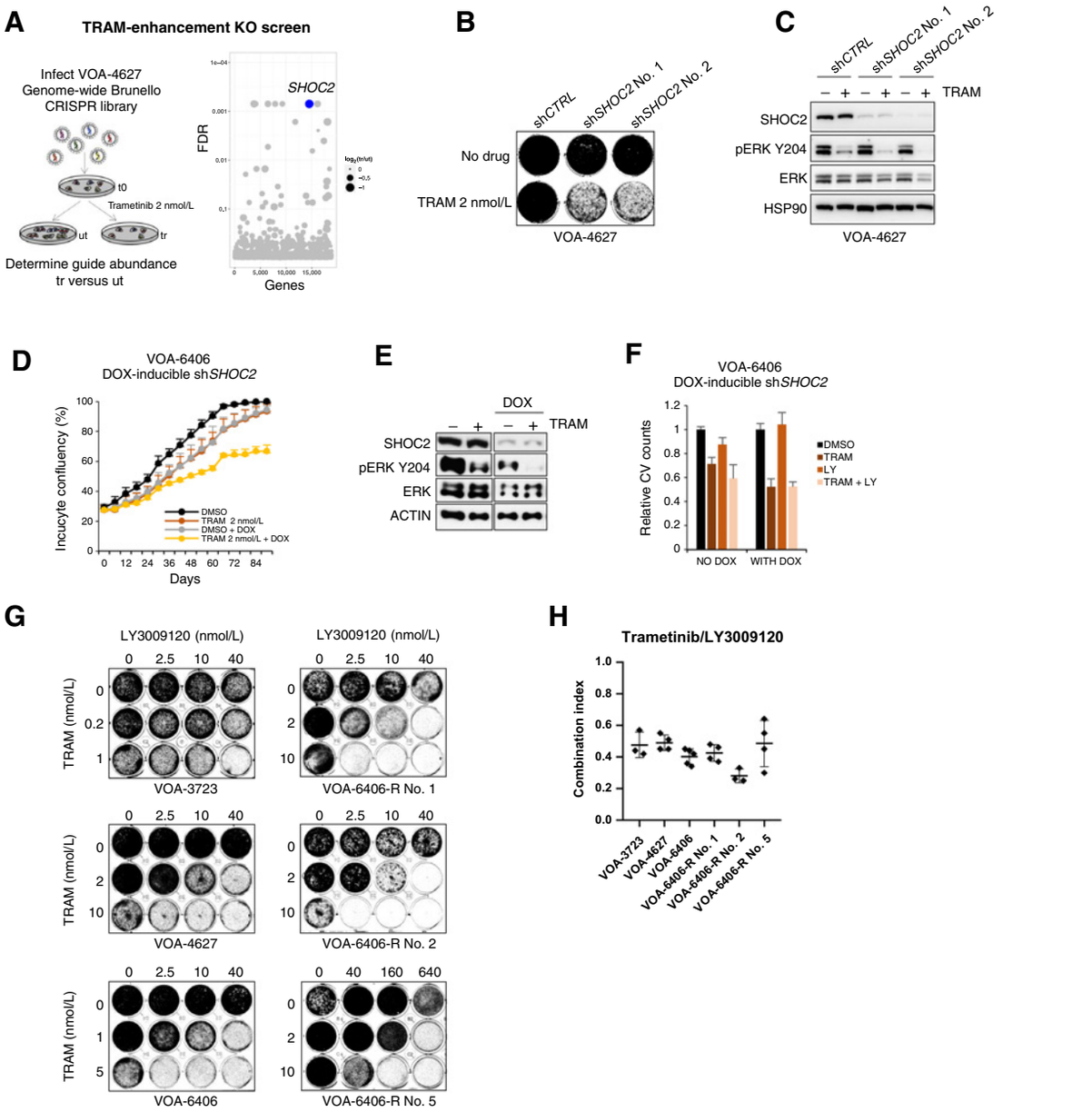

Figure 3.

Genome-wide trametinib enhancer screen identifies *SHOC2*. **A,** Overview of genome-wide trametinib enhancer screen in VOA-4627 cell line with the Brunello library targeting 19,114 genes. Cells were infected with MOI below 0.5 and 1,000× representation of guides. Trametinib selection was performed for 10 days, after which gRNA abundance was determined in treated (tr) over untreated (ut) conditions through deep sequencing. Screens were performed in triplicate. Validated hit *SHOC2* is highlighted in the bubble plot presentation of the RRA MAGeCK analysis. FDR threshold <0.1. **B,** Colony-formation assays were performed with VOA-4627 cells stably infected with sh*CTRL*, sh*SHOC2* No. 1, and sh*SHOC2* No. 2. Plated cells were exposed to 2 nmol/L trametinib concentrations as indicated. The cells were fixed, stained, and scanned after 10 days. **C,** Western blot analysis of total lysates generated from sh*CTRL*, sh*SHOC2* No. 1, and sh*SHOC2* No. 2 VOA-4627 lines exposed to 0 and 10 nmol/L trametinib for 4 days. Blots were probed with the indicated antibodies. HSP90 was used as a loading control. **D,** Cell proliferation assay (IncuCyte) was performed for the doxycycline (DOX) inducible sh*SHOC2* VOA-6406 cell line with the MEKi trametinib (TRAM 2 nmol/L) in the absence or presence of DOX 0.5 μg/mL. **E,** Western blot analysis of total lysates generated from the doxycycline-inducible sh*SHOC2* VOA-6406 cell line (without and with DOX 0.5 μg/mL) exposed to 0 and 2 nmol/L trametinib for 2 days. Blots were probed with the indicated antibodies. ACTIN was used as a loading control. **F,** Cell viability (crystal violet) assay was performed with a doxycycline-inducible sh*SHOC2* VOA-6406 cell line (without and with DOX 0.5 μg/mL) in the presence of the indicated drugs; MEKi trametinib (TRAM, 2 nmol/L), pan-RAF inhibitor (LY3009120, 10 nmol/L) after 4 days of drug exposure. Crystal violet measurements were normalized to their respective DMSO controls. **G,** Colony-formation assays were performed with VOA-3723, VOA-4627, VOA-6406, VOA-6406-R No. 1, VOA-6406-R No. 2, and VOA-6406-R No. 5 with increasing (combination) dosage of trametinib and the pan-RAFi LY3009120 as indicated. The cells were fixed, stained, and scanned after 7 days. **H,** CIs were calculated for the trametinib/LY3009120 combination in a 384-well format normalized to positive (POA) and negative (DMSO) controls. All 384-well growth assays were plated in quadruple and performed multiple times. Displayed are the median CI values of the synergy 5 × 5 concentration matrix. Error bars, SD. CI scores are defined as <0.1 very strong synergism; 0.1–0.3 strong synergism; 0.3–0.7 synergism; 0.7–0.85 moderate synergism; and 0.85–0.9 slight synergism.

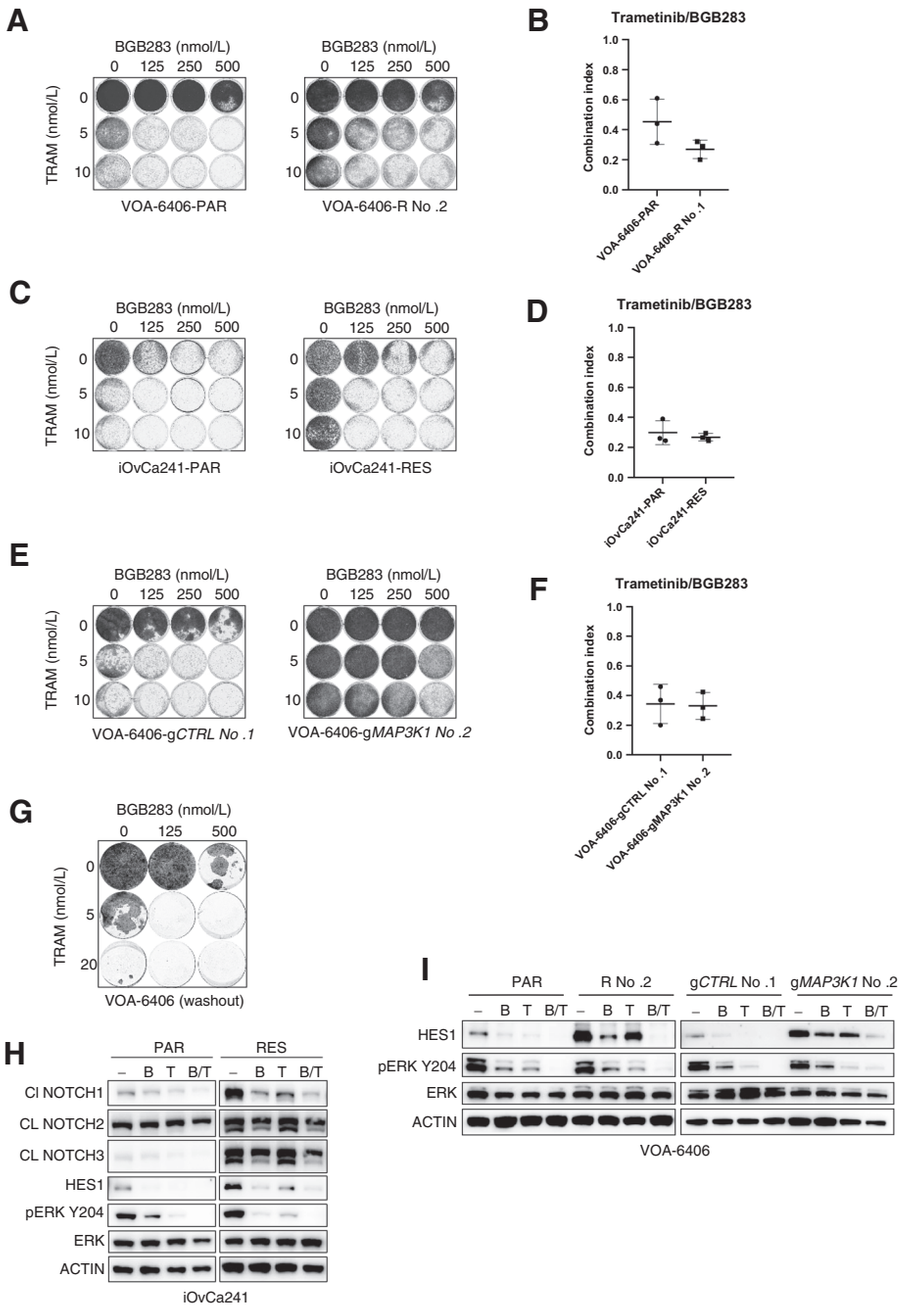

Figure 4.

MEKi/pan-RAFi synergy with the pan-RAFi BGB283. Colony-formation assays and CI calculations were performed for the cell line pairs VOA-6406-PAR and VOA-6406-R No. 2 (**A, B**), iOvCa241-PAR and iOvCa241-RES (**C, D**), and VOA-6406-g*CTRL No. 1* and VOA-6406-g*MAP3K1 No. 2* (**E, F**) with increasing (combination) dosage of trametinib and the pan-RAFi BGB283 as indicated. The cells were fixed, stained, and scanned after 7 days. Colony-formation assays were performed in triplicate, and a representative staining is shown. CIs were calculated for the trametinib/BGB283 combination in 384-well format normalized to positive (POA) and negative (DMSO) controls. All 384-well growth assays were plated in quadruple and performed multiple times. Displayed are the median CI values of the synergy 5 × 5 concentration matrix. Error bars, SD. CI scores are defined as <0.1 very strong synergism; 0.1–0.3 strong synergism; 0.3–0.7 synergism; 0.7–0.85 moderate synergism; and 0.85–0.9 slight synergism. **G,** Colony formation washout experiment with VOA-6406. Cells were exposed to the indicated drugs for 1 week, after which cells were washed and cultured in a normal medium without drugs for 3 weeks. Cells were fixed, stained, and scanned. **H** and **I,** Western blot analyses of total lysates generated from the parental and TRAM-resistant cell line pairs iOvCa241-PAR/RES (H) VOA-6406-PAR/VOA-6406-R No. 2 and VOA-6406 gCTRL No. 1/gMAP3K1 No. 2 (I) exposed to 1 μmol/L BGB283 (B), 10 nmol/L trametinib (T) or the combination (B/T). Blots were probed with the indicated antibodies.

We next sought to extend our findings to PDX LGSOC models. For this, tumor pieces from a *RASG13D*-mutant LGSOC tumor (OC.79) were implanted subcutaneously in NSG mice. The OC.079 model displayed a rather slow growth phenotype and we observed a comparable tumor growth between the control and BGB283 (5 mg/kg) groups. In the trametinib (0.5 mg/kg) group, four of six tumors grew at least twice as large as the start point, whereas in the combination group, four of six tumors showed no obvious tumor growth, with one tumor demonstrating more than 60% tumor reduction (**Fig. 6C** and **D**). Albeit modest, the addition of pan-RAFi enhanced the efficacy of MEKi treatment in this OC.079 PDX model. Due to the slow growing properties, no significant survival benefit was observed in the combination versus control in the 60-day time frame (**Fig. 6E**). The mice tolerated the treatments well, as shown by the small weight loss in these mice (Supplementary Fig. S6B and S6C). In an additional LGSOC PDX model, we were not able to demonstrate a significant benefit of the combination treatment, suggesting that a heterogeneous response to the MEKi/pan-RAFi combination may be expected in the clinic (Supplementary Fig. S6D and S6E). In summary, these observations suggest that pan-RAF inhibition has the potential to sensitize LGSOC models to MEK inhibition suggesting that the MEKi/pan-RAFi combination may be a treatment strategy for a subset of patients with LGSOC.

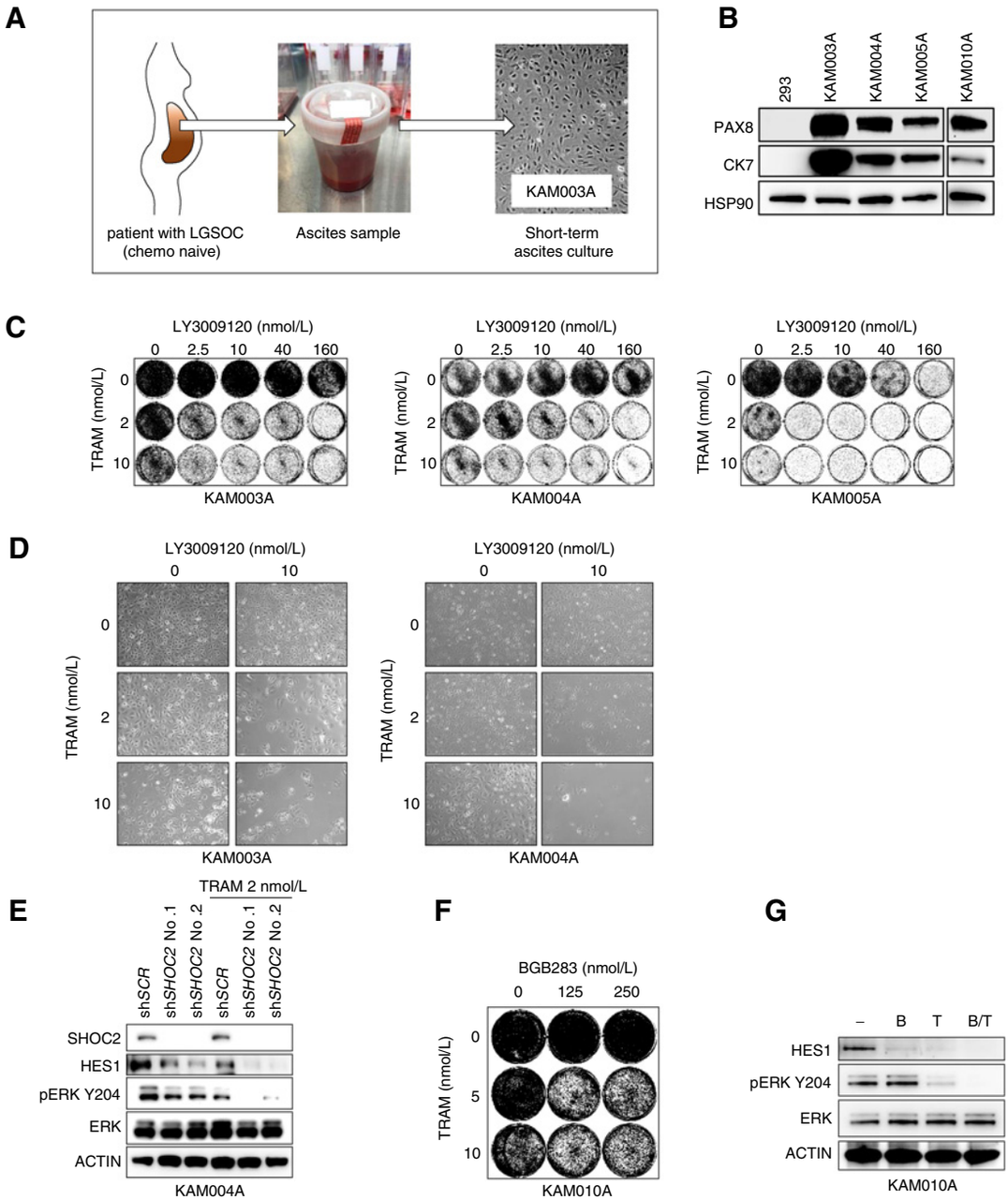

Figure 5.

MEKi/pan-RAFi synergy in primary ascites cultures. **A,** Ascites was retrieved from chemo-naïve patients with LGSOC during debulking surgery or procedures aimed to relieve clinical symptoms. Fresh ascites was directly put in culture flasks yielding a primary ascites culture after 1 to 2 weeks with medium replacement every 3 days. **B,** Western blot analysis of lysates generated from the primary ascites cultures as indicated. Blots were probed with PAX8 or CK7 antibodies. HSP90 was used as a loading control. The 293 cell lysate was used as a negative control. **C,** Long-term colony-formation assays were performed with the primary ascites cultures KAM003A, KAM004A, and KAM005A with increasing (combination) dosage of MEKi trametinib and the pan-RAFi LY3009120 as indicated. The cells were fixed, stained, and scanned after 10 days. **D,** Pictures of the primary ascites cultures KAM003A and KAM004A with indicated (combination) dosage of MEKi trametinib and the pan-RAFi LY3009120 after 10 days. **E,** Western blot of the KAM400A cells infected with sh*SCR* or sh*SHOC2* are probed with the indicated antibodies. **F,** Long-term colony-formation assay was performed with KAM010A with increasing (combination) dosage of MEKi trametinib and pan-RAFi BGB283 as indicated. The cells were fixed, stained, and scanned after 10 days. Colony-formation assays were performed in triplicate, and a representative staining is shown. **G,** KAM010A cells were exposed to 1 μmol/L BGB283 (B), 10 nmol/L trametinib (T) or the combination (B/T) for 2 days, after which lysates were analyzed byWestern blot with the indicated antibodies.

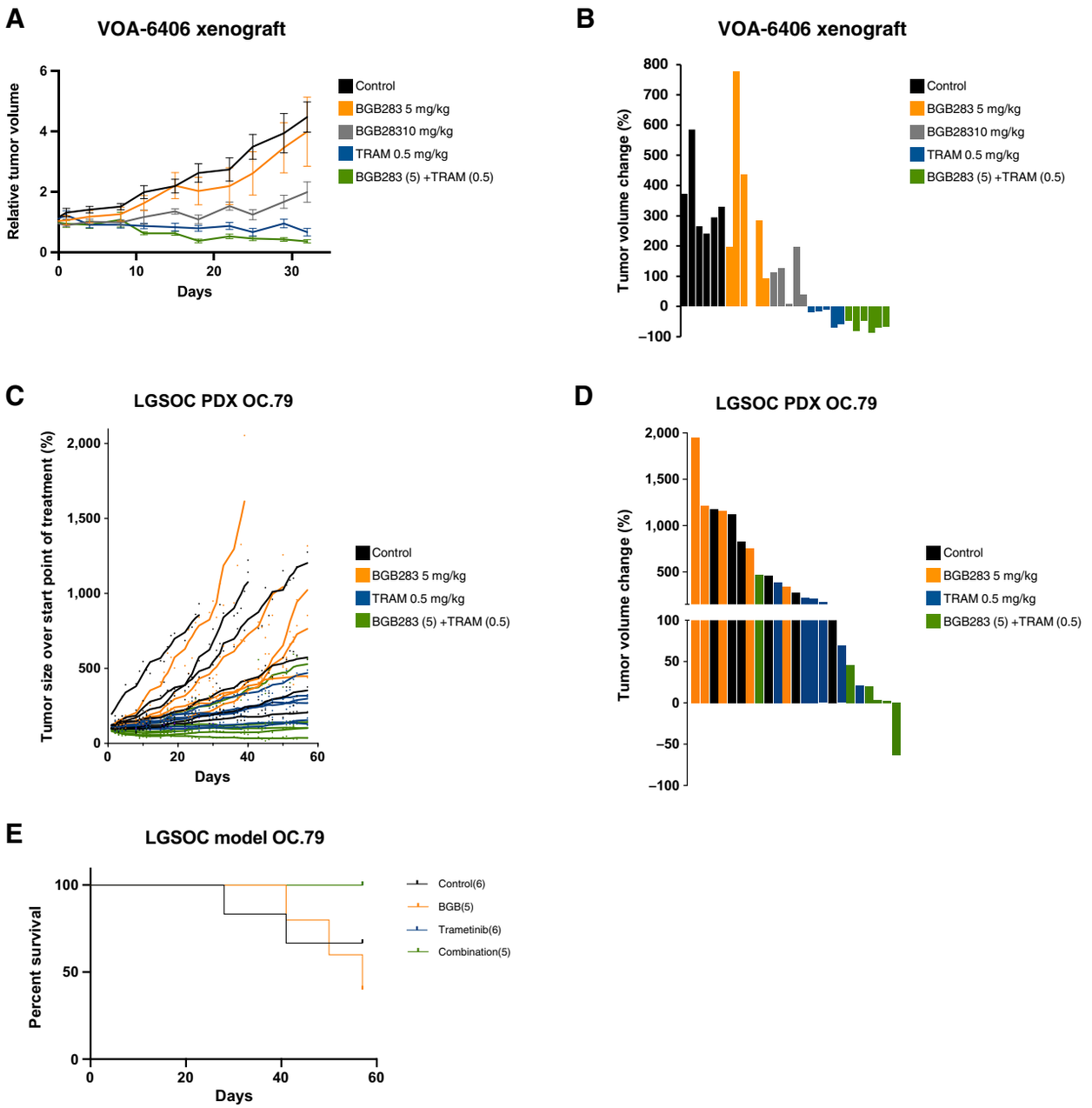

Figure 6.

MEKi/pan-RAFi in the VOA-6406 xenograft and LGSOC PDX mouse model. **A,** VOA-6406 tumors were implanted in NRG mice and treatments (BGB283 5 or 10 mg/kg, trametinib (TRAM) 0.5 mg/kg, BGB283 5 mg/kg + trametinib 0.5 mg/kg) were started when tumors reached 120 mm^3. Shown are relative tumor volumes; error bars, SEM. **B,** Tumor volumes were measured at day 33, and changes in tumor volume compared with baseline (day 0) are indicated. **C,** Relative tumor volumes of the individual tumors of the slow-growing LGSOC PDX model OC.79 (RASG13D-mutant), under the indicated treatments. Treatments were stopped when tumors reached maximum volume (1,500 mm^3) or after 57 days. **D,** Tumor volume changes at the endpoint compared with the start of treatment for the LGSOC PDX model OC.79. **E**, Survival curve for the LGSOC PDX model OC.79.

Discussion

We describe here genome-wide CRISPR/Cas9 screens aimed to identify genes implicated in the response to MEK inhibition in LGSOC.

In MEKi-resistance screens, we identified overexpression of *MAML2* or loss of *MAP3K1* to induce MEKi-resistance. In agreement with its function as a transcriptional coregulator of NOTCH, *MAML2* overexpression resulted in activation of the NOTCH target *HES1*. Activated NOTCH has been described to promote acquired resistance to MAPK inhibitors in both breast cancers and melanomas (38, 39). The identification of the *MAP3K1* hit was an unexpected finding, as we earlier implicated *MAP3K1* loss in increased sensitivity to MEKis in

NSCLC, colon, and breast cancer (40). We suspect that the observed context-dependent effects are caused by the ability of a certain cell type to activate *HES1* transcription upon *MAP3K1* loss. Engagement of NOTCH signaling as the result of *MAP3K1* loss may provide a mechanistic explanation for the tumor suppressor role of *MAP3K1* described in human cancer (41).

In a subset of spontaneous trametinib-resistant VOA-6406 derivatives, we also observed elevated HES1 levels, which appeared critical to the resistance phenotype as both HES1 knockdown or inhibition with JI051 interfered with the trametinib resistance. The induction of HES1 in the resistant clones is probably the consequence of an epigenetic switch as the resistance phenotype appeared reversible. Unfortunately, we could not address the question of whether HES1 induction is solely responsible for trametinib resistance, as we were unable to transiently overexpress HES1 to levels comparable with the resistant subclones. The observation that *HES1* knockdown only partially reversed the resistance suggests that other factors coregulated in the transient switch leading to increased HES1 may be involved in the observed resistance. Interestingly, in both the spontaneous resistant subclones and the *MAP3K1* knockout clones, we observed elevated levels of cleaved NOTCH family members. Collectively, the elevated NOTCH cleavage observed in our trametinib-resistant clones provides an explanation for the induced HES1 transcription.

In the synthetic lethality screen, *SHOC2* loss was shown to enhance MEKi efficacy. This finding was also seen in other cancer types (33, 34). Mimicking SHOC2 inhibition by using the pan-RAFi LY3009120 or BGB283-enhanced trametinib efficacy in multiple LGSOC cell lines, spontaneous trametinib-resistant lines, *in vivo* VOA-6406 xenograft and LGSOC PDX mouse models, as well as freshly established patient with LGSOC ascites cultures. The observed MEKi/pan-RAFi synergy appeared to be independent of *RAS/RAF* mutation status, as only a subset of the responding LGSOC lines have confirmed hotspot *RAS/RAF* mutations. Due to the low numbers, we cannot conclude at this point whether this also holds true for the LGSOC PDX models. Subsequent signaling analysis suggested that the synergistic interaction of MEKi/pan-RAFi cannot solely be explained by enhanced MAPK pathway inhibition. Instead, we suggest that the downregulation of *HES1* transcription upon MEKi/pan-RAFi treatment contributes to the efficient cell arrest by this combination. Similarly, it was recently demonstrated that simultaneous inhibition of NOTCH and MAPK pathway in uveal melanoma enhanced MEKi efficiency by increased MAPK pathway and HES1 downregulation (42).

A recent phase I study on single BGB283 (lifirafenib) treatment reported an acceptable risk–benefit profile and antitumor activity in RAS/RAF mutated solid tumors. This study includes a patient with LGSOC with a durable partial response, emphasizing that the use of the pan-RAFi BGB283 (preferably in combination with trametinib) warrants further testing in LGSOC (43). Furthermore, a complete response with combined MEKi/BRAFi treatment was recently reported for a patient with advanced LGSOC (44), further supporting the notion that targeting the MEK and RAF nodes simultaneously may provide a promising treatment strategy. There may be additional clinical implications to the synergy observed using MEKi/pan-RAFi combinations. MEKi treatment is associated with an unfavorable toxicity profile. Combined MEKi/pan-RAFi treatment may achieve similar or greater efficacy using much lower doses of MEKis, thereby minimizing toxicity.

In summary, through CRISPR/Cas9 screening in LGSOC, we identified that pathways leading to increased *HES1* expression resulted in resistance to the MEKi trametinib. Trametinib combined with pan-RAFi downregulated MAPK and NOTCH signaling, providing an explanation for the observed synergy. Our data indicate that combining trametinib with pan-RAFi may represent a novel treatment strategy for patients with LGSOC.

Authors' Disclosures

S. Li reports grants from the Chinese Scholarship Council during the conduct of the study. G.B.A. Wisman reports grants from the Chinese Scholarship Council during the conduct of the study. S. de Jong reports grants from the Chinese Scholarship Council during the conduct of the study. M.S. Carey reports grants from Canada Research Society/Ovarian Cancer, the Women's Health Research Institute, and the Janet D. Cottrelle Foundation; other support from the BC Cancer Foundation, the VGH and UBC Hospital Foundation, Cure Our Ovarian Cancer during the conduct of the study, Hexamer Therapeutics, aiGENE, Bausch Health, Illumina, Constellation Brands, and Exact Sciences outside the submitted work. K. Berns reports grants from Oncode during the conduct of the study. No disclosures were reported by the other authors.

Authors' Contributions

M. Llaurado Fernandez: Resources, supervision, validation, investigation, visualization, writing–review and editing. **E.M. Hijmans:** Validation, investigation, visualization, writing–review and editing. **A.M.C. Gennissen:** Validation, investigation, visualization, writing–review and editing. **N.K.Y. Wong:** Resources, supervision, validation, investigation, visualization, methodology, writing–review and editing. **S. Li:** Validation, investigation, visualization. **G.B.A. Wisman:** Resources, supervision, writing–review and editing. **A. Hamilton:** Validation, investigation, visualization. **J. Hoenisch:** Validation, investigation, visualization. **A. Dawson:** Validation, investigation. **C.-H. Lee:** Validation, investigation. **M. Bittner:** Validation, investigation, writing–original draft. **H. Kim:** Validation, investigation, visualization. **G.E. DiMattia:** Resources. **C.A.R. Lok:** Resources, validation, writing–original draft. **C. Lieftink:** Data curation, formal analysis, methodology. **R.L. Beijersbergen:** Resources, data curation, formal analysis, supervision, methodology. **S. de Jong:** Resources, supervision, writing–original draft. **M.S. Carey:** Resources, supervision, funding acquisition, writing–original draft. **R. Bernards:** Resources, supervision, funding acquisition, writing–original draft. **K. Berns:** Conceptualization, resources, data curation, formal analysis, supervision, validation, investigation, visualization, methodology, writing–original draft.

Acknowledgments

We are grateful to Inge Vreeswijk-Baudoin and Phuong Le for help with PDX models and to Fiona Zhang for her help with the xenografts. We thank the people from the Genomics Core Facility and the Core Facility Molecular Pathology and Biobanking (CFMPB) of the Netherlands Cancer Institute for their technical support and members of the Bernards lab for their helpful discussions. This research was supported by grants from the Oncode Institute, Chinese Scholarship Council, the Women's Health Research Institute, Cure Our Ovarian Cancer, the Janet D. Cottrelle Foundation, BC Cancer Foundation, Vancouver General/UBC Hospital Foundation, and the MacKenzie, Lawler, MacRae, Ho, Ludemann, and Luther families. Funding was also provided by Health Canada to Ovarian Cancer Canada in support of the OvCAN research initiative.

The publication costs of this article were defrayed in part by the payment of publication fees. Therefore, and solely to indicate this fact, this article is hereby marked "advertisement" in accordance with 18 USC section 1734.

Note

Supplementary data for this article are available at Molecular Cancer Therapeutics Online (http://mct.aacrjournals.org/).

Received January 3, 2022; revised May 30, 2022; accepted October 3, 2022; published first October 5, 2022.

References

1. Gershenson DM. Low-grade serous carcinoma of the ovary or peritoneum. Ann Oncol 2016;27(suppl 1):i45–i49.
2. Singer G, Oldt R, 3rd, Cohen Y, Wang BG, Sidransky D, Kurman RJ, et al. Mutations in BRAF and KRAS characterize the development of low-grade ovarian serous carcinoma. J Natl Cancer Inst 2003;95:484–6.
3. Farley J, Brady WE, Vathipadiekal V, Lankes HA, Coleman R, Morgan MA, et al. Selumetinib in women with recurrent low-grade serous carcinoma of the ovary or peritoneum: an open-label, single-arm, phase 2 study. Lancet Oncol 2013;14: 134–40.
4. Gershenson DM, Sun CC, Bodurka D, Coleman RL, Lu KH, Sood AK, et al. Recurrent low-grade serous ovarian carcinoma is relatively chemoresistant. Gynecol Oncol 2009;114:48–52.
5. Monk BJ, Grisham RN, Banerjee S, Kalbacher E, Mirza MR, Romero I, et al. MILO/ENGOT-ov11: binimetinib versus physician's choice chemotherapy in recurrent or persistent low-grade serous carcinomas of the ovary, fallopian tube, or primary peritoneum. J Clin Oncol 2020;38:3753–62.
6. Gershenson DM, Miller A, Brady WE, Paul J, Carty K, Rodgers W, et al. Trametinib versus standard of care in patients with recurrent low-grade serous ovarian cancer (GOG 281/LOGS): an international, randomised, open-label, multicentre, phase 2/3 trial. Lancet 2022;399:541–53.
7. Berns K, Bernards R. Understanding resistance to targeted cancer drugs through loss of function genetic screens. Drug Resist Updat 2012;15:268–75.
8. Fernandez ML, DiMattia GE, Dawson A, Bamford S, Anderson S, Hennessy BT, et al. Differences in MEKi efficacy in molecularly characterized low-grade serous ovarian cancer cell lines. Am J Cancer Res 2016;6:2235–51.
9. Fernandez ML, Dawson A, Hoenisch J, Kim H, Bamford S, Salamanca C, et al. Markers of MEK inhibitor resistance in low-grade serous ovarian cancer: EGFR is a potential therapeutic target. Cancer Cell Int 2019;19:10.
10. Theriault BL, Portelance L, Mes-Masson AM, Nachtigal MW. Establishment of primary cultures from ovarian tumor tissue and ascites fluid. Methods Mol Biol 2013;1049:323–36.
11. Konermann S, Brigham MD, Trevino AE, Joung J, Abudayyeh OO, Barcena C, et al. Genome-scale transcriptional activation by an engineered CRISPR-Cas9 complex. Nature 2015;517:583–8.
12. Doench JG, Fusi N, Sullender M, Hegde M, Vaimberg EW, Donovan KF, et al. Optimized sgRNA design to maximize activity and minimize off-target effects of CRISPR-Cas9. Nat Biotechnol 2016;34:184–91.
13. Jastrzebski K, Evers B, Beijersbergen RL. Pooled shRNA screening in mammalian cells as a functional genomic discovery platform. Methods Mol Biol 2016;1470: 49–73.
14. Love MI, Huber W, Anders S. Moderated estimation of fold change and dispersion for RNA-seq data with DESeq2. Genome Biol 2014;15:550.
15. Li W, Xu H, Xiao T, Cong L, Love MI, Zhang F, et al. MAGeCK enables robust identification of essential genes from genome-scale CRISPR/Cas9 knockout screens. Genome Biol 2014;15:554.
16. Jin H, Shi Y, Lv Y, Yuan S, Ramirez CFA, Lieftink C, et al. EGFR activation limits the response of liver cancer to lenvatinib. Nature 2021;595:730–4.
17. Chou TC. Drug combination studies and their synergy quantification using the Chou-Talalay method. Cancer Res 2010;70:440–6.
18. Khan ZM, Real AM, Marsiglia WM, Chow A, Duffy ME, Yerabolu JR, et al. Structural basis for the action of the drug trametinib at KSR-bound MEK. Nature 2020;588:509–14.
19. Peng SB, Henry JR, Kaufman MD, Lu WP, Smith BD, Vogeti S, et al. Inhibition of RAF isoforms and active dimers by LY3009120 leads to anti-tumor activities in RAS or BRAF mutant cancers. Cancer Cell 2015;28:384–98.
20. Tse C, Shoemaker AR, Adickes J, Anderson MG, Chen J, Jin S, et al. ABT-263: a potent and orally bioavailable Bcl-2 family inhibitor. Cancer Res 2008;68: 3421–8.
21. Tang Z, Yuan X, Du R, Cheung SH, Zhang G, Wei J, et al. BGB-283, a novel RAF kinase and EGFR inhibitor, displays potent antitumor activity in BRAF-mutated colorectal cancers. Mol Cancer Ther 2015;14:2187–97.
22. Perron A, Nishikawa Y, Iwata J, Shimojo H, Takaya J, Kobayashi K, et al. Small-molecule screening yields a compound that inhibits the cancer-associated transcription factor Hes1 via the PHB2 chaperone. J Biol Chem 2018;293: 8285–94.
23. Poratti M, Marzaro G. Third-generation CDK inhibitors: a review on the synthesis and binding modes of palbociclib, ribociclib and abemaciclib. Eur J Med Chem 2019;172:143–53.
24. Akinleye A, Furqan M, Mukhi N, Ravella P, Liu D. MEK and the inhibitors: from bench to bedside. J Hematol Oncol 2013;6:27.
25. Maira SM, Stauffer F, Brueggen J, Furet P, Schnell C, Fritsch C, et al. Identification and characterization of NVP-BEZ235, a new orally available dual phosphatidylinositol 3-kinase/mammalian target of rapamycin inhibitor with potent in vivo antitumor activity. Mol Cancer Ther 2008;7:1851–63.
26. Luistro L, He W, Smith M, Packman K, Vilenchik M, Carvajal D, et al. Preclinical profile of a potent gamma-secretase inhibitor targeting notch signaling with in vivo efficacy and pharmacodynamic properties. Cancer Res 2009;69:7672–80.
27. Morohashi Y, Kan T, Tominari Y, Fuwa H, Okamura Y, Watanabe N, et al. C-terminal fragment of presenilin is the molecular target of a dipeptidic gamma-secretase-specific inhibitor DAPT (N-[N-(3,5-difluorophenacetyl)-L-alanyl]-S-phenylglycine t-butyl ester). J Biol Chem 2006;281:14670–6.
28. Alkema NG, Tomar T, Duiker EW, Jan Meersma G, Klip H, van der Zee AG, et al. Biobanking of patient and patient-derived xenograft ovarian tumour tissue: efficient preservation with low and high fetal calf serum-based methods. Sci Rep 2015;5:14495.
29. Suddason T, Gallagher E. A RING to rule them all? Insights into the Map3k1 PHD motif provide a new mechanistic understanding into the diverse roles of Map3k1. Cell Death Differ 2015;22:540–8.
30. Groenendijk FH, de Jong J, Fransen van de Putte EE, Michaut M, Schlicker A, Peters D, et al. ERBB2 mutations characterize a subgroup of muscle-invasive bladder cancers with excellent response to neoadjuvant chemotherapy. Eur Urol 2016;69:384–8.
31. Wang H, Daouti S, Li WH, Wen Y, Rizzo C, Higgins B, et al. Identification of the MEK1(F129L) activating mutation as a potential mechanism of acquired resistance to MEK inhibition in human cancers carrying the B-RafV600E mutation. Cancer Res 2011;71:5535–45.
32. Diaz-Padilla I, Wilson MK, Clarke BA, Hirte HW, Welch SA, Mackay HJ, et al. A phase II study of single-agent RO4929097, a gamma-secretase inhibitor of Notch signaling, in patients with recurrent platinum-resistant epithelial ovarian cancer: a study of the Princess Margaret, Chicago and California phase II consortia. Gynecol Oncol 2015;137:216–22.
33. Sulahian R, Kwon JJ, Walsh KH, Pailler E, Bosse TL, Thaker M, et al. Synthetic lethal interaction of SHOC2 depletion with MEK inhibition in RAS-driven cancers. Cell Rep 2019;29:118–34.
34. Jones GG, Del Rio IB, Sari S, Sekerim A, Young LC, Hartig N, et al. SHOC2 phosphatase-dependent RAF dimerization mediates resistance to MEK inhibition in RAS-mutant cancers. Nat Commun 2019;10:2532.
35. Vakana E, Pratt S, Blosser W, Dowless M, Simpson N, Yuan XJ, et al. LY3009120, a panRAF inhibitor, has significant anti-tumor activity in BRAF and KRAS mutant preclinical models of colorectal cancer. Oncotarget 2017;8:9251–66.
36. Klein ME, Kovatcheva M, Davis LE, Tap WD, Koff A. CDK4/6 inhibitors: the mechanism of action may not be as simple as once thought. Cancer Cell 2018;34: 9–20.
37. Iavarone C, Zervantonakis IK, Selfors LM, Palakurthi S, Liu JF, Drapkin R, et al. Combined MEK and BCL-2/XL inhibition is effective in high-grade serous ovarian cancer patient-derived xenograft models and BIM levels are predictive of responsiveness. Mol Cancer Ther 2019;18:642–55.
38. Martz CA, Ottina KA, Singleton KR, Jasper JS, Wardell SE, Peraza-Penton A, et al. Systematic identification of signaling pathways with potential to confer anticancer drug resistance. Sci Signal 2014;7:ra121.
39. Krepler C, Xiao M, Samanta M, Vultur A, Chen HY, Brafford P, et al. Targeting Notch enhances the efficacy of ERK inhibitors in BRAF-V600E melanoma. Oncotarget 2016;7:71211–22.
40. Xue Z, Vis DJ, Bruna A, Sustic T, van Wageningen S, Batra AS, et al. MAP3K1 and MAP2K4 mutations are associated with sensitivity to MEK inhibitors in multiple cancer models. Cell Res 2018;28:719–29.
41. Pham TT, Angus SP, Johnson GL. MAP3K1: genomic alterations in cancer and function in promoting cell survival or apoptosis. Genes Cancer 2013;4: 419–26.
42. Porcelli L, Mazzotta A, Garofoli M, Di Fonte R, Guida G, Guida M, et al. Active notch protects MAPK activated melanoma cell lines from MEK inhibitor cobimetinib. Biomed Pharmacother 2021;133:111006.
43. Desai J, Gan H, Barrow C, Jameson M, Atkinson V, Haydon A, et al. Phase I, open-label, dose-escalation/dose-expansion study of lifirafenib (BGB-283), an RAF family kinase inhibitor, in patients with solid tumors. J Clin Oncol 2020;38: 2140–50.
44. Tholander B, Koliadi A, Botling J, Dahlstrand H, Von Heideman A, Ahlstrom H, et al. Complete response with combined BRAF and MEK inhibition in BRAF mutated advanced low-grade serous ovarian carcinoma. Ups J Med Sci 2020;125: 325–9.